Nanoscopic Insight into Water Adsorption and Desorption in Commercial Activated Alumina by Positron Annihilation Lifetime Spectroscopy

Wojciech Kowalski , Mateusz Kochel , Agnieszka Kierys , Marek Gorgol , Marek Drewniak , Radosław Zaleski *

Posted Date: 2 July 2025

doi: 10.20944/preprints202507.0193.v1

Keywords: activated alumina;water adsorption and desorption;positron annihilation;drying

 doi:10.20944/preprints202507.0193.v1

Article

Nanoscopic Insight into Water Adsorption and Desorption in Commercial Activated Alumina by Positron Annihilation Lifetime Spectroscopy

Wojciech Kowalski [1], Mateusz Kochel [2], Agnieszka Kierys [3], Marek Gorgol [4], Marek Drewniak [3] and Radosław Zaleski [4,*]

[1] Faculty of Mathematics, Physics and Computer Science, Maria Curie-Skłodowska University, 1 Maria Curie-Skłodowska Square, 20-031 Lublin, Poland
[2] Department of Circular Economy, Institute of Energy and Fuel Processing Technology, Zamkowa 1, 41-803 Zabrze, Poland
[3] Institute of Chemical Sciences, Maria Curie-Skłodowska University, 3 Maria Curie-Skłodowska Square, 20-031 Lublin, Poland
[4] Institute of Physics, Maria Curie-Skłodowska University, 1 Maria Curie-Skłodowska Square, 20-031 Lublin, Poland
* Correspondence: radek@zaleski.umcs.pl

Abstract

Activated alumina is widely used in industry as an adsorbent. Its strong affinity toward water allows for the profound dehydration of gas streams. To optimize such processes, a deeper insight into water interaction with activated alumina is required. This knowledge can be obtained using positron annihilation lifetime spectroscopy, a sensitive tool that unravels previously unknown aspects of adsorption processes. Activated alumina (Compalox® AN/V-813) was subjected to such a study supported by detailed characterization using scanning electron microscopy, X-ray diffraction, and N_2 adsorption-desorption. A complex porous structure of the material, consisting mainly of boehmite and η-Al_2O_3 or γ-Al_2O_3, was found. It is responsible for significant differences in adsorption and desorption. The course of adsorption is close to the classical layer-by-layer description. However, there are indications of initial water capture at active sites and final water reorganization consisting of filling the smallest free volumes that remain empty. The narrow mesopore inlets that keep water in the pores even at a relative vapor pressure of 0.4 are primarily responsible for the course of the desorption process. During adsorption, water is mainly maintained in the form of small clusters up to the highest pressures, whereas during desorption, it is continuous until narrow pore openings.

Keywords: activated alumina; water adsorption and desorption; positron annihilation; drying

1. Introduction

Activated alumina is a porous, inorganic adsorbent distinguished by its high specific surface area, low degree of crystallinity, and abundance of surface-active sites. Its excellent mechanical strength, remarkable thermal and chemical stability, and relatively low production costs have made it a material of enduring interest for a wide range of industrial applications [1]. Structurally, it is partially amorphous and is dominated by mesopores of varied geometry. Due to its amphoteric nature, alumina exhibits both acidic and basic surface properties simultaneously [2]. The presence of surface hydroxyl (–OH) groups imparts strong polarity, which plays a key role in molecular interactions. At the same time, coordinatively unsaturated acidic sites act as highly reactive centers capable of attaching nucleophilic species.

 doi:10.20944/preprints202507.0193.v1

In industrial practice, activated alumina is typically produced by thermally dehydrating aluminum hydroxide precursors, most commonly gibbsite, boehmite, or pseudo-boehmite. Depending on the calcination conditions and the type of precursor used, activated alumina can adopt various crystalline forms, including the stable α-alumina polymorph (corundum) or one of several metastable or transitional phases (η, γ, χ, δ, κ, and θ) [3]. In adsorption applications, the transitional phases γ-Al_2O_3, χ-Al_2O_3, and – less commonly – η-Al_2O_3 are crucial due to their high porosity. Variations in the structure and phase composition of these forms result in distinct adsorption mechanisms, porosity profiles, and surface properties, significantly affecting the material's interactions with water [4]. In practice, however, commercial alumina adsorbents rarely have a single phase. Instead, they tend to be mixtures, with various phases and surface groups coexisting and interacting – an aspect increasing the complexity of the adsorption system.

Thanks to its unique properties, activated alumina is widely used in industry as an adsorbent, catalyst, and catalyst support. As an adsorbent, it is commonly applied for drying gases and liquids [5–7], removing polar contaminants from hydrocarbon streams [8], and desulfurizing liquid fuels [9]. Additionally, it is employed in water and wastewater treatment for the adsorption of trace amounts of fluoride [10–12], arsenic [13,14], and organic dyes [15,16]. Among all these applications, gas drying remains one of the most important and widespread uses of activated alumina. Its strong affinity towards polar molecules, such as water, allows for the profound dehydration of gas streams. Combined with high mechanical strength and chemical resistance, this makes activated alumina particularly well-suited for use in cyclic systems, such as temperature and pressure swing adsorption.

Optimizing adsorption processes requires more than a general understanding of the material – it demands in-depth knowledge of the adsorbent itself, its surface structure, and the properties and mechanisms determining the course of adsorption and desorption. Activated alumina presents a particularly complex case, with a multifaceted structure and a wide variety of chemical surface groups [17,18]. Water adsorption on this material proceeds through a combination of physical mechanisms, including hydrogen bonding and capillary condensation, as well as chemical interactions involving the dissociation of water molecules and the formation of surface-bound hydroxyl (–OH) groups. Notably, the process initiates at very low relative pressures (p/p_0). The resulting adsorption isotherm typically shows type IV characteristics with a distinct hysteresis loop [19], reflecting the intricate dynamics of water retention and release.

Hysteresis in adsorption-desorption cycles cannot be explained solely by capillary condensation or irreversible evaporation. Surface-related effects and the clustering of water molecules also play a significant role [17]. Adsorption may proceed via coordinative and dissociative mechanisms [20]. The hydroxyl groups that form on the surface are significant, as they enable the buildup of additional, more loosely bound layers of water, which may eventually lead to condensation in larger mesopores [21]. Pore filling and emptying is a nuanced process governed by both the chemical character of the surface and the interactions between adsorbate and surface, many aspects of which remain not fully understood [22]. Unraveling these mechanisms requires a broad analytical perspective and the use of complementary research techniques.

In this context, several well-established methods are widely employed to investigate the structure and properties of porous materials, including activated alumina. Commonly used methods include, among others, low-temperature nitrogen adsorption/desorption isotherms analysis [23,24], FTIR spectroscopy [25], X-ray diffraction [26], nuclear magnetic resonance [27,28], transmission electron microscopy [26], and scanning electron microscopy. Each technique offers a different perspective on the material's properties and comes with its limitations. As a result, gaining a comprehensive understanding of adsorption phenomena often requires combining multiple analytical tools. Classical approaches, such as low-temperature nitrogen adsorption and mercury intrusion porosimetry, remain the standard practice regarding pore structure analysis. Nitrogen-based measurements of pore filling and emptying can provide valuable structural insights. However, their accuracy at the lower limit of pore sizes is sometimes insufficient. In addition, the results obtained with this method may be distorted due to the interaction of nitrogen molecules with the

 doi:10.20944/preprints202507.0193.v1

adsorbent, e.g., artificially opening pores that would otherwise be closed. [29]. Altogether, such limitations emphasize the need to broaden the scope of characterization methods and to integrate complementary techniques for a more reliable interpretation of experimental data [22].

In recent years, positron annihilation lifetime spectroscopy (PALS) has emerged as a highly sensitive and flexible tool for probing a broad spectrum of porous materials. These include porous systems with diverse free volume characteristics, such as zeolites [30–33], metal-organic frameworks (MOFs) [34], porous polymers [35], various forms of silica-based materials [36,37], and composites [38]. Positrons exhibit an exceptional sensitivity to various free volumes, i.e., spaces with zero electron density. This includes closed and open pores, interfacial regions, and voids where ortho-positronium (o-Ps) can be trapped. One of the significant advantages of PALS lies in its ability to perform in situ measurements under changing process conditions without altering the sample or disturbing the processes [39–43]. This makes it particularly well-suited for precisely characterizing porous materials and extracting reliable data on process flow. When combined thoughtfully with complementary methods, such as X-ray diffraction or scanning electron microscopy, PALS offers insights into adsorption mechanisms that are often inaccessible through conventional approaches.

Although the scientific literature on alumina and its metastable phases is extensive, fundamental studies that shed light on adsorption and desorption mechanisms at the nanoscale are still relatively limited, especially regarding commercial adsorbent materials. These materials are typically complex mixtures of multiple crystalline phases, which makes their analysis significantly more challenging. Furthermore, they often contain various additives derived from proprietary manufacturing processes, further complicating the interpretation of experimental findings. Despite widespread industrial use and research of activated alumina, many aspects of its surface structure and adsorption behavior remain only partially understood. The material's structural complexity and the diversity of its surface chemical groups continue to make it a complex system to fully characterize, particularly at the molecular level [27,44]. A deeper insight into interactions between water molecules and the surface of activated alumina could help improve the optimization of adsorption processes in practical, real-world industrial applications. Therefore, this work provides insight into the details of water adsorption in a commercially available and commonly used activated alumina.

2. Materials and Methods

2.1. Material

Activated alumina (Compalox® AN/V-813, Martinswerk GmbH [45]) in the form of low-dust grains with a size of 1-3 mm was obtained from ABC-Z System EKO s.c., Poland. The grains were powdered in a mortar before all experiments.

2.2. Characterization

The microstructure of the activated alumina powder surface (after gold-palladium sputtering) was observed using a scanning electron microscope (SEM, FEI Company, Quanta 3D FEG) working at an accelerating voltage of 5 kV. An energy-dispersive X-ray spectrometer (EDS) coupled with the same microscope, working at 20 kV, was used to determine the elemental composition of the sample.

The X-ray diffraction (XRD) pattern of powdered Al_2O_3 was recorded using an Empyrean X-ray diffractometer (PANalytical, Malvern, UK) equipped with CuKα radiation (λ = 0.154 nm). The data was collected in the 2θ range of 20° to 100° and referenced against the ICDD PDF4+ 2023 database.

The parameters characterizing the porosity of the powdered activated alumina were determined from N_2 adsorption-desorption at −196 °C using a volumetric adsorption analyzer (ASAP 2020 V4.01, Micromeritics, Norcross, GA). Before the measurement, the sample was degassed at 200 °C for 1000 minutes. The specific surface area (S_{BET}) was calculated based on N_2 adsorption data using the standard Brunauer − Emmett − Teller (BET) equation [23], while the total pore volume (V_p) was estimated from single-point adsorption at a relative pressure of about 0.99. The pore size distribution (PSD) was determined from the N_2 adsorption branch of the isotherm using the Density Functional

 doi:10.20944/preprints202507.0193.v1

Theory (DFT) method. The DFT analysis was performed using the Micromeritics MicroActive v1.01 software, assuming of nitrogen adsorption on an oxide surface and alternatively a cylindrical or slit pore shape.

2.3. Water Adsorption and Desorption

Adsorption and desorption of water on the activated alumina were monitored with positron annihilation lifetime spectroscopy (PALS). Photons with energy of 1275 keV, which accompany positron creation inside a 120 kBq ^{22}Na radioactive source, enclosed inside an 8 μm thick Kapton® envelope, and photons with energy of 511 keV from positron/positronium annihilation inside the investigated sample were collected with two scintillation detectors (Scionix), equipped with BaF_2 scintillators. The pulses from photomultipliers were processed with an Agilent U1065A digitizer (Acqiris) at a sampling rate of 4 GS/s and then analyzed with dedicated software [46], which enabled the determination of the time differences between 1275 keV ("start") and 511 keV ("stop") signals. The PALS spectra were collected in short time intervals (ca. 10 minutes) during the entire adsorption/desorption procedure, and then the spectra counts collected during the stable pressure level were summed to obtain statistics sufficient for numerical analyses. The LT_92 program [47] was primarily used for the analysis of all spectra. Total counts in each spectrum were in the range of 8.5 to 9.5 million. Source contribution was set to 10% of total intensity, with a lifetime of 0.382 ns. A single Gaussian with a typical FWHM of 0.204 ns ± 0.003 ns was used as a resolution function. Selected spectra were analyzed with the MELT program [48]. It provided continuous lifetime distributions, which were transformed into PSDs using positron porosimetry equations [49].

The pressure control was assured by the setup schematically presented in Figure A1 (Appendix). After placing the sample and positron source in the measurement chamber, the spectrometer was started. The chamber pressure was reduced to below 1 Pa using a rotary vane pump and then further decreased to ca. 10^{-4} Pa with a turbomolecular pump for thorough cleansing at room temperature. This process took about 3 days, as indicated by the stabilized PAL spectra. The chamber was then isolated, and distilled water vapor (Milli-Q, 5 MΩ cm at 298 K) was introduced through a gas gauge. Before introduction, the water was degassed three times using freeze-pump-thaw cycling.

The chamber was incrementally filled with water vapor, with pressure levels increasing every 12 hours by ca. 0.05 p_0 (saturated water vapor pressure at ambient temperature, 295 K ± 1 K). The "inlet" gas gauge was dynamically regulated through software for 30 minutes at the start of each step, assuring a constant pressure during water adsorption. Then, after closing the valves, a pressure drop was observed for some time, indicating ongoing adsorption. The PAL spectra from the time of valve opening and pressure stabilization were discarded. After reaching p_0 and stabilizing the PAL spectra, the water reservoir was sealed off. Desorption was initiated by decreasing the pressure with the "outlet" gas gauge (through a fully open "inlet" gas gauge) in 12-hour intervals each time by ca. 0.1 p_0, analogously to adsorption. When the pressure stabilization level became < 0.03 p_0, continuous vacuum pumping was initiated using a rotary pump. After the next 40 h, when the pressure decreased below 1.5 Pa, a turbomolecular pump was started and continued pumping for ca. 29 h.

Finally, after completing the desorption run, the chamber with the sample was filled with water vapor in three steps at different pressure levels and then, analogously, evacuated in three steps, with manual control over the gauges. During this procedure, the PALS spectra were collected to verify if the measured pressure was affected by air leakage during the previous long-lasting adsorption-desorption cycle.

 doi:10.20944/preprints202507.0193.v1

3. Results and Discussion

3.1. Characterization

The SEM micrographs of the surface of activated alumina powder (Figure 1) show that milling of Compalox® AN/V-813 grains results in the formation of small, irregularly shaped pieces. Their structure appears to be composed of plate-like forms or sheets that are relatively tightly packed, but that easily fall apart when grinding, breaking into smaller fragments. The EDS spectrum of activated alumina powder (Figure A2, Appendix) contains peaks that can be attributed to oxygen, aluminum, sodium, and carbon (Figure 1). The calculated amount of oxygen is (52±2) wt% / (60±4) at%, aluminium (39±3) wt% / (27±3) at%, sodium (0.29±0.03) wt% / (0.24±0.02) at% and carbon is approx. (8±4) wt% / (13±6) at%. It is worth noting that the amount of light elements, including carbon, cannot be precisely determined by SEM-EDS. The presence of sodium is consistent with the producer information [45]. A carbon (C) peak is always visible, even though a specimen under study does not contain carbon, due to the carbon film that is used as a carrier in SEM-EDS. However, considering the XRD result (Figure 2), the presence of carbon should not be treated solely as an artifact. Although the method of production of Compalox® activated alumina is not disclosed and still is secret know-how, it cannot be ruled out that carbon is formed because of contamination from used chemical reagents, including precursors or some organic additives. The addition of such agents was indicated, for example, in patents [50–52].

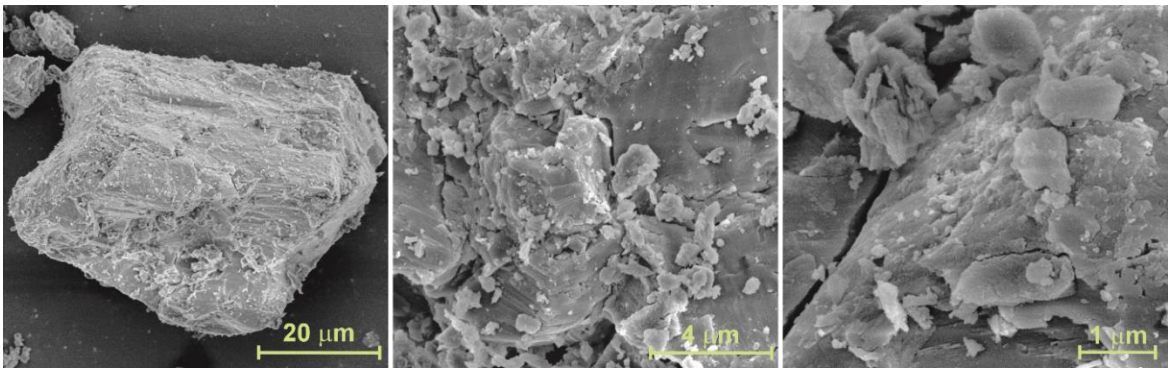

Figure 1. SEM micrographs of activated alumina powder at different magnifications.

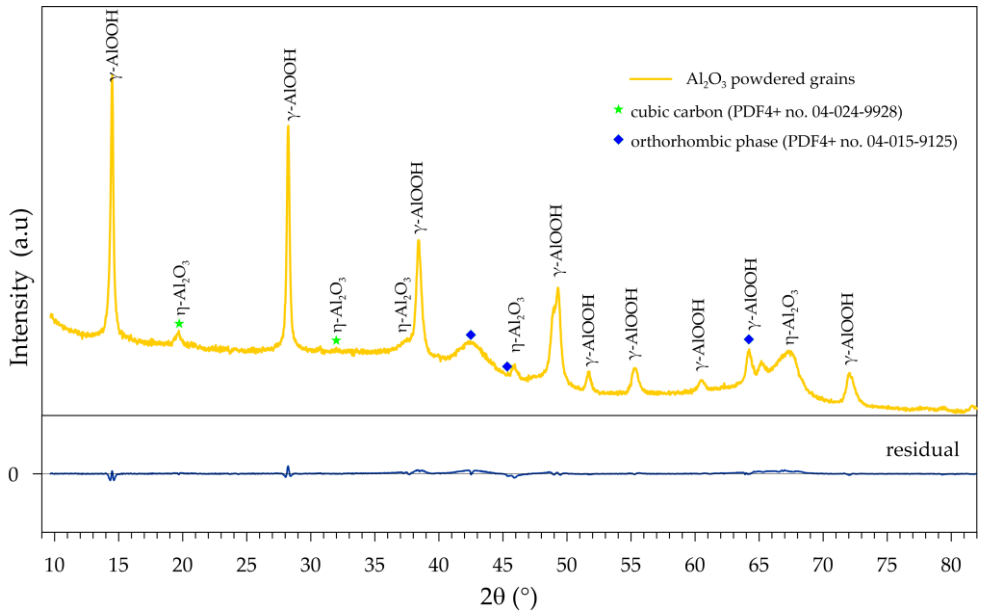

Figure 2. XRD pattern of activated alumina powder.

 doi:10.20944/preprints202507.0193.v1

Determining the phase composition of activated alumina was not an easy task, as the investigated material turned out to have a complex composition. The XRD pattern is dominated by diffraction reflexes at 2θ values of 14.5°, 28.2°, 38.3°, 48.9°, and 55.2°, which correspond well with the pattern of aluminum oxyhydroxide γ-AlOOH (boehmite) (PDF4+ no. 04-10-5684). The boehmite (which accounts for ca. 64%) is accompanied by alumina, which has a cubic crystal structure with the Fd-3m space group, as relatively small reflexes can be distinguished at 2θ values of 37.7°, 45.9°, as well as at 66.9°, and most importantly, at 19.4°. The presence of the latter signal is a subtle difference in the XRD powder patterns of γ- and η-Al_2O_3 but makes it possible to distinguish these two phases from each other, as postulated by Zhou and Snyder [53]. Therefore, this additional phase, which constitutes about 33%, could be considered eta-alumina (η-Al_2O_3, PDF4+ no. 04-007-2615). However, considering the complex nature of the XRD pattern of the investigated activated alumina, the presence of γ-Al_2O_3 phase instead of η-Al_2O_3 cannot be excluded. Additionally, the precise crystalline structure of the γ-Al_2O_3 phase remains a topic of scientific debate [54,55], with various structural models proposed, including a cubic structure. Nevertheless, the assumption of only boehmite and η-Al_2O_3, or only γ-Al_2O_3, in the investigated sample does not provide a satisfactory fit to the measured XRD. A much better fit is obtained by additionally assuming the presence of cubic carbon (PDF4+ no. 04-024-9928) and a second additional orthorhombic crystalline phase (for example, PDF4+ no. 04-015-9125). The presence of the latter phase, whose content is below 3%, is evidenced by a broad and low-intensity diffraction signal at a 2θ value of 42.5°. The presence of carbon cannot be ruled out, considering the EDS results and those provided by the manufacturer; however, its presence should be treated with great caution, and its content is certainly low (less than 1%).

The nitrogen adsorption/desorption isotherms are shown in Figure 3a. The adsorption isotherm seems to exhibit a combination of type I and type II isotherms of the IUPAC classification [56], suggesting the coexistence of micropores and large mesopores in the activated alumina structure. The hysteresis loop most closely resembles the H4 type and exhibits a sharp step-down in the desorption branch at about $p/p_0 \sim 0.45$, which can be attributed to cavitation-induced evaporation. It can, therefore, be assumed that there are free volumes in the activated alumina under study in the shape of an ink bottle with a narrow neck and a wide body part.

The information on the PSD was derived from the adsorption branch of isotherm by applying the DFT method with an assumption of either cylindrical (Figure 3b) or slit shape (Figure 3c) of pores. Regardless of the pore shape, the obtained PSD indicates the presence of a group of small mesopores with sizes below 5 nm (PSD with the maximum at 2.9 nm or 3.2 nm when the cylindrical shape or slit shape of pores is assumed, respectively). The DFT method that assumes a cylindrical pore shape corresponds to the model used in the PALS method, which allows for a comparison of the results from both methods. However, considering the phase composition of the sample, it seems more appropriate to assume a slit-like shape of the pores in the DFT model.

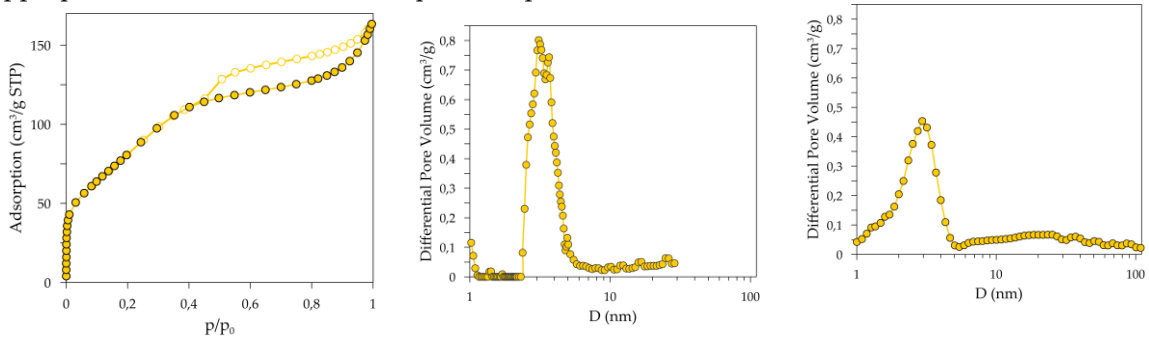

(**a**) (**b**) (**c**)

Figure 3. N_2 adsorption/desorption isotherms (**a**) and pore size distributions of activated alumina powder determined by the DFT method with an assumption of the cylindrical (**b**) and slit shape (**c**) of pores. The lines are provided for convenience.

 doi:10.20944/preprints202507.0193.v1

3.2. Water Adsorption and Desorption

The MELT analysis of the dry-activated alumina spectrum (Figure 4a, relative water vapor pressure $p/p_0 = 0$) reveals the existence of six components with different lifetimes. They originate from para-positronium (p-Ps, lifetime < 0.2 ns), positrons that annihilate without forming a Ps state (e^+, lifetime ca. 0.4 ns), and ortho-positronium (o-Ps, four components with lifetimes > 1 ns). The large number of o-Ps components indicates a complex porous structure, with the PSD of two long-lived components (Figure 5a, $p/p_0 = 0$) corresponding to the distribution obtained from N_2 adsorption/desorption isotherms and presented in Figure 3b. The shift of positron porosimetry results towards smaller sizes indicates that the parameter value $\Delta = 0.166$ nm may be too low for characterizing activated alumina pores, and model calibration is desirable [57,58]. However, since the main subject of this work is the study of water adsorption, for which this parameter value is the most appropriate [59], it will be retained in further calculations of positron porosimetry results. The intermediate-lived components, i.e., with lifetimes of the order of several nanoseconds, correspond to smaller (sub-nanometer) free volumes in the activated alumina structure. They most likely originate from the trapping of o-Ps at the crystal grain boundaries, whose diversity and significant concentration are expected due to the coexistence of different phases in the material (Figure 2).

The trend of changes in individual components of PALS spectra was followed by comparing the results for a series of spectra at different stages of water adsorption (Figure 4a):

- dry ($p/p_0 = 0$),
- approximately in the middle of mesopore filling ($p/p_0 = 0.50$),
- pores almost filled ($p/p_0 = 1.00$),

and then desorption (Figure 4b):

- empty mesopores start to appear ($p/p_0 = 0.44$),
- approximately in the middle of mesopore emptying ($p/p_0 = 0.30$),
- pores almost completely emptied ($p/p_0 = 0.02$).

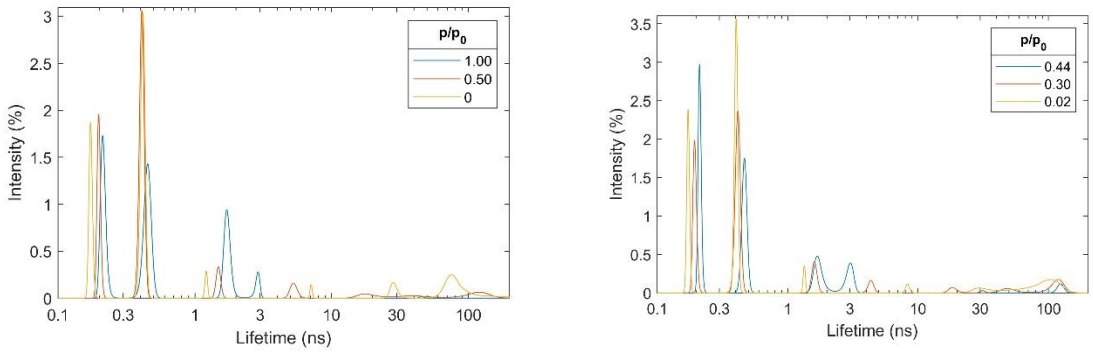

(**a**) (**b**)

Figure 4. Positron lifetime distribution obtained using MELT for subsequent stages of water adsorption (**a**) and desorption (**b**) from activated alumina powder.

The p-Ps lifetime changes significantly with the relative pressure of water p/p_0 (i.e., with the amount of water adsorbed). In the dry material, it has a value of 0.17 ns (Figure 4a), which is quite a large value for porous oxides. A value greater than 0.125 ns, expected for intrinsic p-Ps annihilation, may indicate an admixture of positron (not forming positronium) annihilation in the dislocations of the alumina crystal structure [60]. During adsorption, this value gradually increases to over 0.21 ns, which is characteristic of water [61], where numerous radiation processes occur that affect the lifetime of p-Ps [62,63]. During desorption, an analogous change occurs in the opposite direction.

Also, the lifetime of long-lived (compared to alumina defects) positrons not bound in Ps changes with the relative pressure of water. However, in this case, the increase in its lifetime from 0.40 ns to over 0.45 ns is visible only when long-lived components (related to mesopores) disappear. This is

 doi:10.20944/preprints202507.0193.v1

also observed in both adsorption and desorption cases. The change in this lifetime may also be related to radiation processes, which do not affect the lifetimes of positrons as long as the thermalizing positron releases energy in water clusters separated from those in which its annihilation occurs [64], i.e., until pores are filled with a continuous water volume. It is also possible that this change results from a distortion of this component due to the inclusion of part of the grain boundary annihilation, as described later.

The changes in o-Ps lifetimes (> 1 ns) and the shape of their distributions are easier to discuss after transforming them into PSDs (Figure 5). However, it should be remembered that such an operation results in minor discrepancies from the actual distributions, which arise from the simplified assumptions that all pores have the same cylindrical shape and their walls are made of the same material (while they may be covered with water). An easily noticeable and reversible change is that the peaks of the size distribution in the sub-nanometer size range (D < 1 nm) come closer together during adsorption and move apart during desorption. The decrease in the size of the micropores, from almost 1 nm to 0.5-0.6 nm, can be simply explained by the location of more and more water molecules (which are smaller than 0.3 nm) within them, which reduces the space available for o-Ps. The explanation for the increase in the size of the space at the grain boundaries from 0.3 nm to 0.4 nm is somewhat more complex. The origin of this component changes as the volume of water in the pores increases. Individual water clusters become so large that o-Ps bubbles can form inside them. The bubbles are spaces that normally do not exist in liquids but are created as a result of the equilibrium between the surface tension of the liquid and the zero energy of o-Ps, which "pushes" the surrounding molecules [65]. Annihilation at grain boundaries still occurs, but its probability is much lower than that of annihilation in bubbles. It can no longer be isolated as a separate component due to its small intensity and a similar lifetime to the "bubble" component. The lifetime and size of the bubbles in fully hydrated activated alumina (Figures 4a and 5a, $p/p_0 = 1$) are slightly smaller than in bulk water. This indicates the proximity of the walls, which limits the growth of bubbles and/or the interaction of the walls with water molecules. This latter is particularly likely due to the numerous -OH groups in boehmite. Both sub-nanometer free volume groups return to their initial sizes upon desorption. It is worth noting that during desorption (change between p/p_0 of 1.0 in Figure 5a and 0.44 in Figure 5b), a visible decrease in the number of o-Ps bubbles (area under the peak at 0.40 nm drops ca. two times) at a constant micropore volume (area under the peak at 0.55 nm remains appx. constant) is visible. This means that the micropores are the last to empty.

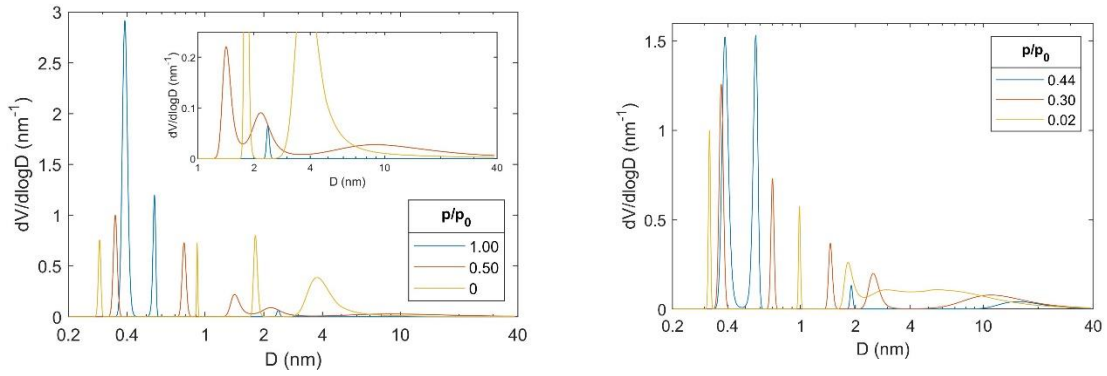

(**a**) (**b**)

Figure 5. Pore size distributions obtained using positron porosimetry from MELT's o-Ps lifetime distributions for subsequent stages of water adsorption (**a**) and desorption (**b**) from activated alumina powder.

The already wide and complex mesopore size distribution is further widened during water adsorption (Figure 5a, $p/p_0 = 0.50$). The apparent bimodal PSD is shifted towards smaller sizes (1.8 nm → 1.4 nm and 3.8 nm → 2.2 nm). This suggests that the pore walls are covered with a layer of water, which limits the free space inside them. This differs from the course in similarly sized cylindrical silica pores [66], where "plugs" were formed instead of a layer of water on the walls. This

 doi:10.20944/preprints202507.0193.v1

may be due to the predominance of the forces binding water to the pore walls over the forces of interaction between water molecules. The appearance of an additional, very wide peak with a maximum of about 9 nm, covering nearly the entire mesopore range, is responsible for the broadening of the whole pore distribution. Its appearance can be attributed to the reduced probability of o-Ps trapping in smaller pores and the higher efficiency of positronium formation on the surface covered with a water layer than on alumina. In turn, after filling the pores with water, a small peak remains in the PSD around 2.4 nm. It probably comes from a small group of closed pores. Given the low intensity of the component from which it originates, both its position and width are subject to very high uncertainty.

The evolution of the mesopore size distribution during desorption proceeds in a classical manner. First, next to the closed pores with a size of ca. 1.9 nm, the largest pores (D > 10 nm with the PSD maximum at 15 nm) appear (Figure 5b, $p/p_0 = 0.44$), the distribution of which widens (D > 5 nm with the PSD maximum at 11 nm) with a decrease in the relative water vapor pressure ($p/p_0 = 0.30$). At the same time, free volumes appear in pores whose walls are covered with water, as shown by the restored bimodal distribution with peaks at 1.5 nm and 2.5 nm. As a result, the distribution is very similar to that during adsorption (Figure 5a, $p/p_0 = 0.50$) but at a much lower pressure, $p/p_0 = 0.30$. At the end of water removal ($p/p_0 = 0.02$), the PSD resembles the initial one in dry activated alumina, but it is much broader. It can be suspected that this result is due to the inaccuracy of the MELT analysis, which does not reproduce broad distributions well [67]. However, it is also possible that the narrow distribution observed before water introduction was due to pore size averaging by migrating positronium in the interconnected pore network [38]. In this case, the wide pore distribution would mean that despite the low p/p_0, not all connections between mesopores were unblocked.

To follow the course of adsorption and desorption, PALS spectra measured at successive pressures, changing with a small pressure step, were investigated. The analysis of lifetime distributions would not be legible due to the large number of results. Therefore, a simplified analysis model was used, assuming the presence of 5 - 6 components with lifetimes without distributions. This significantly reduced the uncertainty of the results and made it easier to track changes in the spectra with the water vapor pressure. Two short-lived components, which correspond to (1) p-Ps and (2) positrons that have not formed Ps, do not provide additional information beyond that discussed in the analysis of the MELT results (i.e., distributions of lifetimes and free volumes). Therefore, we will focus only on components 3 - 6 originating from the o-Ps annihilation. Since the formation, trapping, and annihilation of o-Ps, which are considered in the positron porosimetry models, can be influenced by various additional effects (e.g. the already mentioned change in the material forming the pore walls [42] and o-Ps migration [68]) converting lifetimes and intensities to pore sizes and volumes could be misleading. Therefore, further interpretation of the adsorption and desorption process will be carried out using primary parameters obtained from the PALS spectra, i.e., lifetimes (τ_n) and intensities (I_n), where n = 3, 4, 5, 6.

The results of the analysis using a simplified PALS spectra model (Figure 6) show that the most distinct changes are visible in the intensities of the individual components, which is why they will be mainly used to discuss the observed process. The 6th component provides information about the largest pores. It is usually assumed that its intensity (I_6) is primarily related to the total pore surface area or concentration at a given pore size. However, it may also depend to some extent on connections with smaller pores, from where additional o-Ps may flow, as well as the difference in the probability of o-Ps formation on free volume walls composed of different materials (e.g., η-Al_2O_3, γ-AlOOH, water). During adsorption, the change of I_6 occurs in almost the entire pressure range, ranging from the predominant value in the spectrum of about 13% to almost zero. However, the main sigmoidal decrease is observed in the p/p_0 range between 0.3 and 0.7. An analogous change in the opposite direction occurs during desorption, but it is sharper and covers a lower and much narrower range of p/p_0, i.e., 0.4 - 0.2. The simplified model provides imprecise information about τ_6, as the dispersion of its values exceeds any noticeable trend.

 doi:10.20944/preprints202507.0193.v1

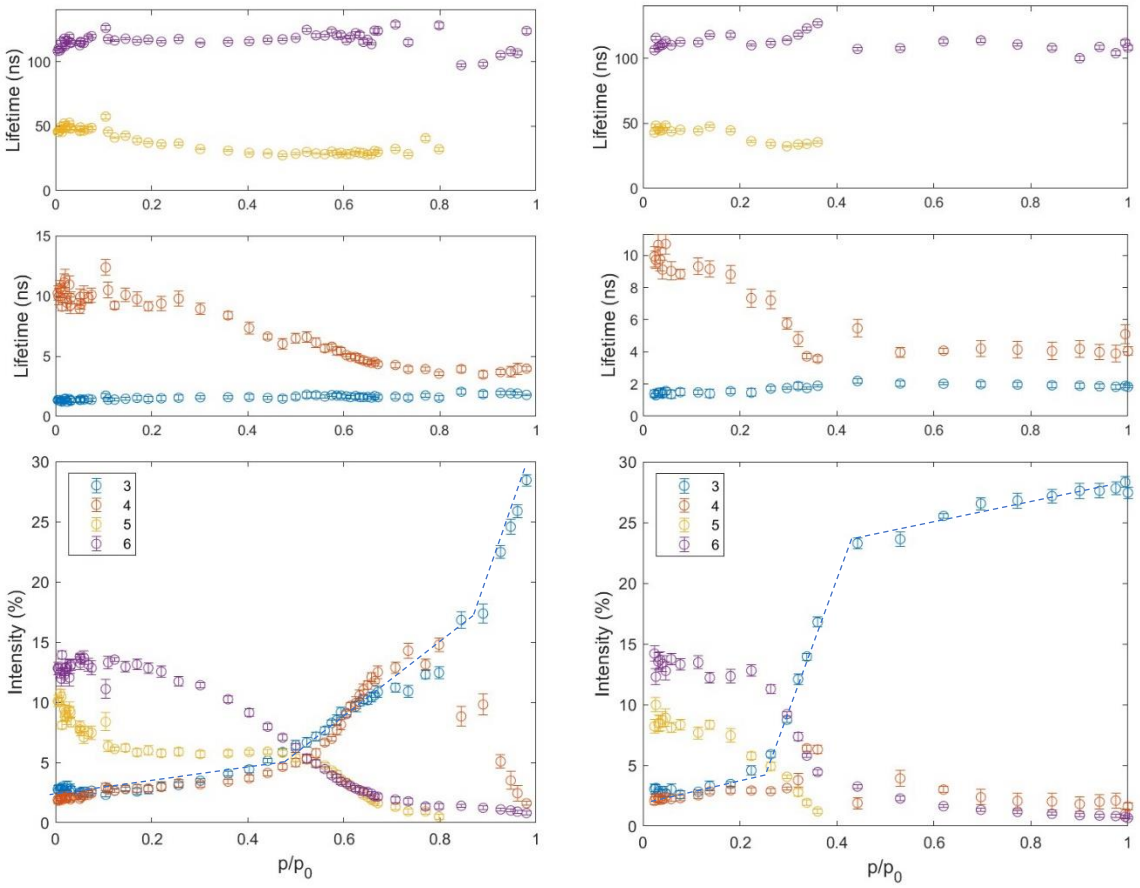

(**a**) (**b**)

Figure 6. Lifetimes and intensities of o-Ps components (3-6) determined by LT as a function of relative water vapor pressure during adsorption (a) and desorption (b) from activated alumina powder. Dashed lines are eye-guides.

Otherwise, for the 5th component, the decrease in lifetime is clear. This confirms the observations presented during the analysis of MELT results, i.e., covering the walls of several-nanometer-sized mesopores with water. Whereas, the different course of I_5 from I_6 is somewhat surprising. Already in the pressure range of 0 - 0.1, it is almost halved from its initial value of about 10%. This decrease in I_5 can be attributed to the occupancy of active sites, which significantly participate in the formation of positronium, e.g., functional groups, with water molecules. Such an effect may be absent in the case of component 6 because pores from group 5, with dimensions of 2 nm, occur in a different form of material (see Figure 2) than larger pores from group 6. However, it should be remembered that o-Ps annihilating in the large mesopores of group 6 is most likely formed in micropores, which most likely have a different wall structure (e.g., due to their small size). Interestingly, the low-pressure effect of increasing I_5 does not occur during desorption, which may indicate a permanent change in the character of the pore surface due to interaction with water.

At $p/p_0 > 0.1$, I_5 stabilizes while I_6 systematically decreases. This may indicate that the small mesopores of group 5 have blocked inlets and are inaccessible to water below a certain threshold pressure, which can push condensed water through the blocked inlets. This type of pore shape is sometimes referred to as an “ink bottle”. However, it is also possible that these pores are too large for capillary condensation in this p/p_0 range, while “micropore driven” I_6 decreases due to condensation

 doi:10.20944/preprints202507.0193.v1

(or rather "clogging") in micropores even smaller than those of group 5. The term "capillary condensation" may be misleading for possibly slit pores of group 5. This shape would additionally justify relatively high condensation pressure for group 5 mesopores, i.e., p/p_0 of about 0.5, above which I_5 decreases almost identically to I_6. Above p/p_0 of 0.8, the intensities of both components are so small that they cannot be distinguished with satisfactory accuracy, and a single component is used to approximate them both. During desorption, although the increase in I_5 occurs in parallel with I_6, it maintains a significantly lower value in contrast to adsorption. This discrepancy between I_5 and I_6 is consistent with typical capillary evaporation, when large mesopores of group 6 are emptied before small mesopores of group 5. However, the increase of I_6 occurs at much lower pressure than its decrease during adsorption. This can be explained if some of the large pores of group 6 can be emptied only through the narrow inlets of small mesopores of group 5. Nevertheless, some shifts in the emptying pressure can also be related to the different shapes of group 5 and 6 pores.

In the micropores, represented by the 4th component, the size of the voids also changes significantly with increasing pressure, as reflected by a significant decrease in lifetime (τ_4). Interestingly, this change very closely reproduces the changes in I_6 in both the adsorption and desorption cases. This is a premise to consider that the migration of o-Ps [37] formed in the larger micropores is the main source of the high I_6, i.e., o-Ps annihilating in the largest free volumes. This provides an alternative explanation for the previous interpretation of the shift of the increase in I_6 toward low pressures during desorption due to the narrow inlets of group 5 pores. The decrease in τ_4 during adsorption is accompanied by a gradual increase in I_4, from about 2% to its doubling at p/p_0 of about 0.5. Then, I_4 increases up to 15%, followed by its stabilization in the p/p_0 range of 0.7-0.8, and then decreases to zero at the saturated vapor pressure. This change can be attributed to the relative nature of the o-Ps intensities; i.e., the initial increase in I_4 could result from the decrease in I_5 and I_6, while the decrease is due to the predominant probability of o-Ps formation in water (i.e., I_3, which will be discussed later). However, comparing this result with earlier studies on water and alkane adsorption in silicas and polymers [41,42,66,69], it can be expected that this is an effect of the formation of a gap at the interface between water and alumina. The surprising difference from the other materials is that the size of this gap is much larger in alumina. Again, this suggests a significantly different interaction of water with alumina (understood as boehmite / η-Al_2O_3 / γ-Al_2O_3). This can also indicate a significantly different (rougher) surface topography, which may consist of micropore inlets and grain boundaries. The gap is greatly reduced at $p/p_0 > 0.9$ after the rearrangement of water molecules or a change in the chemical nature of the alumina surface. The latter effect may be consistent with the lack of low-pressure changes in I_5, which were observed at the beginning of adsorption and at the final stage of water removal. During desorption, the I_4 increase effect, which can be observed at p/p_0 of about 0.35, is much weaker, if present at all.

The interpretation of the shortest-lived 3rd o-Ps component is quite unambiguous compared to other components. As already mentioned, its initial origin from the free volumes on the grain boundaries changes to o-Ps bubbles. Such bubbles can only form when the water clusters have a sufficiently large volume. Therefore, this component does not convey information about the presence of water molecules in the sample, but rather about the formation of its clusters larger than the o-Ps bubble, i.e., 0.5 nm. Nevertheless, the 3rd component carries very clear and useful information about the course of water adsorption and desorption, as well as the differences between the course of water condensation and evaporation. During adsorption, three distinct ranges can be identified, each with an approximately linear increase in I_3, albeit at a different rate. Below a relative pressure of about 0.5 p/p_0, there are practically no water clusters, and the increase in I_3 results rather from a decrease in the other intensities. In the range of 0.5-0.9 p/p_0, the volume of water capable of containing an o-Ps bubble increases approximately linearly. This indicates the filling of subsequent pores, the merging of small water clusters into larger ones, etc. Finally, the rapid increase in I_3 at $p/p_0 > 0.9$ most likely indicates the merging of separated water volumes, but also the disappearance of space allowing o-Ps to locate at the water-solid interface.

 doi:10.20944/preprints202507.0193.v1

The course of desorption is fundamentally different from that of adsorption, reflecting hysteresis not so much in the amount of water but in the transition from its dispersed to continuous form and vice versa. For most of the pressure range, down to p/p_0 of about 0.4, I_3 decreases very slightly, indicating that confined water remains in a continuous form with almost no loss. Below this pressure, a relatively rapid drop in I_3 occurs. At p/p_0 of about 0.25, it reaches a value characteristic of free spaces at grain boundaries, indicating that water has dispersed and is unable to accommodate o-Ps bubbles. This type of very wide hysteresis seems to confirm the ink-bottle shape of pores. Comparing the pressure values at which the I_3 drop occurred with the PALS desorption study in silica [66], the pore inlet sizes can be estimated at 2-3 nm. This would point out the group 5 pores, but the different interaction of water with alumina than with silica may distort this value. Finally, important information about the pore structure is provided by the lack of bubble size growth (i.e., τ_3) during desorption, which would be expected due to the occurrence of negative pressure in the pores [40]. Such behavior is characteristic of strongly connected pores with narrow inlets, which confirms the previous interpretation of the course of the adsorption and desorption process.

5. Conclusions

Standard methods of material characterization indicate that the structure of the Compalox® activated alumina is relatively closely packed and composed of plate-like forms or sheets. It consists mainly of boehmite, accompanied most probably by η-Al_2O_3. However, the presence of a small admixture of other phases cannot be excluded. Both micropores and large mesopores are present in the structure of activated alumina, arranged in a manner that facilitates cavitation-induced nitrogen evaporation, such as the ink-bottle structure.

Positron annihilation lifetime spectroscopy provided a unique insight into the course of adsorption and desorption. Although the interpretation of the results is not direct and requires reconstructing the phenomena leading to the annihilation of positronium, placing it in the context of previous research allows us to understand details of the course of the studied processes that are otherwise inaccessible.

The general course of water adsorption in activated alumina was determined by positron porosimetry at several characteristic water vapor pressures. Unlike in cylindrical silica pores, where water “plugs” are formed during adsorption, a layer of water forms on the walls of alumina, limiting the free space inside the pores. This may indicate a different ratio of the force binding water to the pore walls and the force of interaction between water molecules in alumina than in silica. Desorption, like adsorption, proceeds in the manner described by the classical picture. The largest empty spaces appear first, and their distribution expands as the relative water vapor pressure decreases. However, positron porosimetry allows us to conclude that at the end of desorption, not all connections between mesopores are unblocked.

In turn, monitoring adsorption and desorption by PALS in fine pressure steps reveals additional details of water confinement in the pores of activated alumina. Initially, water molecules adsorb on active sites in smaller mesopores. This suppresses o-Ps formation, testifying that these sites are rich in weakly bonded electrons. Further capillary condensation in smaller mesopores occurs at a relative water vapor pressure characteristic of the pore size, considering that their shape may resemble slits. The correct interpretation of PALS results is possible thanks to the knowledge that o-Ps, while annihilating in the largest mesopores, most likely forms in much smaller micropores. On this basis, a picture emerges that during adsorption, micropores are systematically blocked already from low pressures, resulting in the inhibition of the migration of o-Ps from micropores to the largest mesopores. However, the micropores are only filled when water is pushed into them just below the saturated water vapor pressure. This may be due to the strong binding of water to the functional groups close to their inlets. Then the water also merges into a continuous volume, previously remaining mainly in the form of isolated clusters. This can be particularly interesting in technical applications, e.g., requiring a large surface area of water, and it is difficult to determine using any other method than PALS. This continuous volume of water is present over most of the pressure range

 doi:10.20944/preprints202507.0193.v1

during desorption, with no signs of cavitation. The subsequent changes in free volumes suggest that larger mesopores can only empty through relatively narrow inlets that become unblocked only at low pressures.

The material collected in this study can be used to optimize the use of Compalox® activated alumina. However, above all, it is worth emphasizing its importance for further interpretations of water adsorption results on other materials. Similarly, previous water and alkane adsorption studies performed for various adsorbents helped to interpret the results presented in this work.

Author Contributions: Conceptualization, M.K. and R.Z.; methodology, R.Z.; software, W.K., and R.Z.; validation, W.K., M.G., A.K., and R.Z.; formal analysis, W.K., A.K., M.D., and R.Z.; investigation, M.G., W.K., A.K., and M.D.; resources, M.K.; data curation, W.K., M.G., A.K., and M.D.; writing—original draft preparation, W.K., M.K., A.K., M.G., and R.Z.; writing—review and editing, W.K., M.K., A.K., M.G., and R.Z.; visualization, W.K., A.K., and R.Z.; supervision, R.Z.; project administration, R.Z. All authors have read and agreed to the published version of the manuscript.

Funding: This research received no external funding.

Institutional Review Board Statement: Not applicable.

Informed Consent Statement: Not applicable.

Data Availability Statement: The dataset is available on request from the authors.

Acknowledgments: The authors would like to thank ABC-Z System EKO s.c. for providing the sample for research and Katarzyna Zaleska for providing space for Radosław Zaleski to work on this article.

Conflicts of Interest: The authors declare no conflicts of interest.

Abbreviations

The following abbreviations are used in this manuscript:

BET	Brunauer – Emmett – Teller equation
DFT	Density functional theory
EDS	Energy dispersive X-ray spectrometer
PALS	Positron annihilation lifetime spectroscopy
PSD	Pore size distribution
SEM	Scanning electron microscope
XRD	X-ray diffraction

Appendix

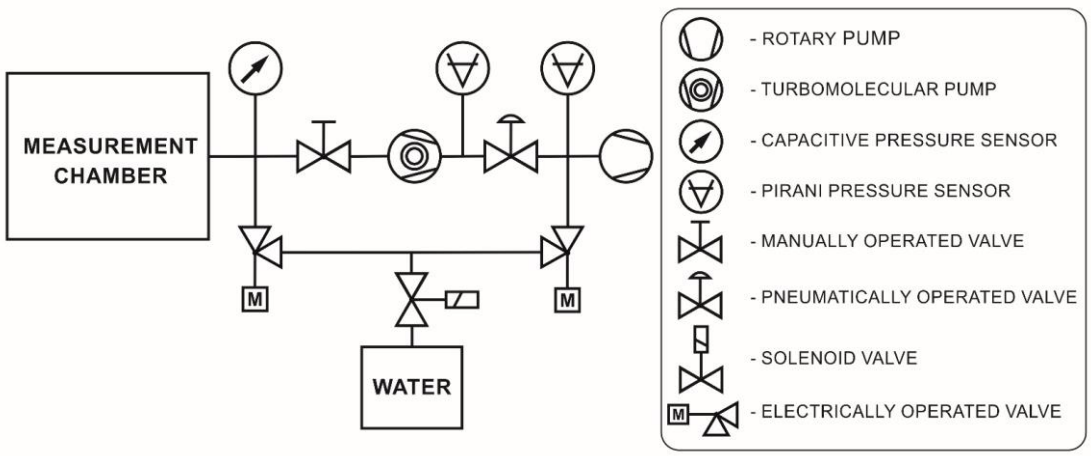

Figure A1. Schematics of the pressure system dedicated to the water adsorption-desorption measurements.

 doi:10.20944/preprints202507.0193.v1

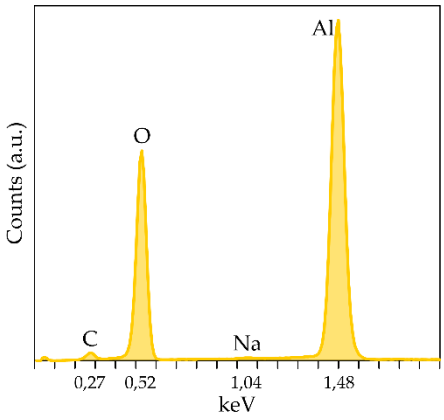

Figure A2. EDS spectrum of activated alumina powder.

References

1. Yang, R. T., *Adsorbents: Fundamentals and Applications*. John Wiley & Sons: 2003; p 424.
2. Digne, M.; Sautet, P.; Raybaud, P.; Euzen, P.; Toulhoat, H., Use of DFT to achieve a rational understanding of acid–basic properties of γ-alumina surfaces. *J. Catal.* **2004,** 226, (1), 54-68.
3. Levin, I.; Brandon, D., Metastable Alumina Polymorphs: Crystal Structures and Transition Sequences. *J. Am. Ceram. Soc.* **1998,** 81, (8), 1995-2012.
4. Kasprzyk-Hordern, B., Chemistry of alumina, reactions in aqueous solution and its application in water treatment. *Adv. Colloid Interface Sci.* **2004,** 110, (1-2), 19-48.
5. Oh, H.-T.; Lim, S.-J.; Kim, J. H.; Lee, C.-H., Adsorption Equilibria of Water Vapor on an Alumina/Zeolite 13X Composite and Silica Gel. *J. Chem. Eng. Data* **2017,** 62, (2), 804-811.
6. Reshetnikov, S.; Kurzina, I., Investigation of adsorption of water vapor on porous aluminium oxide material. *IOP Conference Series: Materials Science and Engineering* **2019,** 597, (1), 012011.
7. Hong, S.-H.; Jin, S.; Ho, K.; Hur, E.; Lee, C.-H., Adsorption Equilibria of Water Vapor on Surface-Modified Activated Carbons and Alumina. *J. Chem. Eng. Data* **2019,** 64, (11), 4834-4843.
8. Saha, D.; Deng, S., Characteristics of Ammonia Adsorption on Activated Alumina. *J. Chem. Eng. Data* **2010,** 55, (12), 5587-5593.
9. Srivastav, A.; Srivastava, V. C., Adsorptive desulfurization by activated alumina. *J. Hazard. Mater.* **2009,** 170, (2-3), 1133-1140.
10. De Paula, N.; Maraschin, M.; Knani, S.; De Oliveira, J. T.; Agustini, C. B.; Féris, L. A.; Claussen, L. E.; De Souza, D. M.; Oliveira, M. L. S.; Silva, L. F. O.; Dotto, G. L.; Jahn, S. L.; Carissimi, E., Ozone-treated activated alumina as an alternative adsorbent to remove fluoride from water: Conventional and Bayesian approaches to evaluate the isotherms, kinetics, and thermodynamics. *Journal of Environmental Chemical Engineering* **2023,** 11, (6), 111403.
11. Hu, C. Y.; Lo, S. L.; Kuan, W. H., Effects of the molar ratio of hydroxide and fluoride to Al(III) on fluoride removal by coagulation and electrocoagulation. *J. Colloid Interface Sci.* **2005,** 283, (2), 472-476.
12. Zamorategui Molina, A.; Ramírez Ramírez, N.; Martínez Rosales, J. M.; Serafín M, A. H., Síntesis y caracterización de gamma alúmina y su comparación con un carbón activado para remover el fluoruro presente en agua potable de pozos. *Acta Universitaria* **2016,** 26, (2), 30-35.
13. Inchaurrondo, N.; Di Luca, C.; Mori, F.; Pintar, A.; Žerjav, G.; Valiente, M.; Palet, C., Synthesis and adsorption behavior of mesoporous alumina and Fe-doped alumina for the removal of dominant arsenic species in contaminated waters. *Journal of Environmental Chemical Engineering* **2019,** 7, (1), 102901.
14. Giles, D. E.; Mohapatra, M.; Issa, T. B.; Anand, S.; Singh, P., Iron and aluminium based adsorption strategies for removing arsenic from water. *Journal of Environmental Management* **2011,** 92, (12), 3011-3022.
15. Fernandes, E. P.; Silva, T. S.; Carvalho, C. M.; Selvasembian, R.; Chaukura, N.; Oliveira, L. M. T. M.; Meneghetti, S. M. P.; Meili, L., Efficient adsorption of dyes by γ-alumina synthesized from aluminum wastes: Kinetics, isotherms, thermodynamics and toxicity assessment. *Journal of Environmental Chemical Engineering* **2021,** 9, (5), 106198.

 doi:10.20944/preprints202507.0193.v1

16. Ali, S.; Abbas, Y.; Zuhra, Z.; Butler, I. S., Synthesis of γ-alumina (Al2O3) nanoparticles and their potential for use as an adsorbent in the removal of methylene blue dye from industrial wastewater. *Nanoscale Advances* **2019,** 1, (1), 213-218.
17. Viisanen, Y.; Lbadaoui-Darvas, M.; Alvarez Piedehierro, A.; Welti, A.; Nenes, A.; Laaksonen, A., Water Vapor Adsorption–Desorption Hysteresis Due to Clustering of Water on Nonporous Surfaces. *Langmuir* **2024,** 40, (38), 20311-20321.
18. Ionescu, A.; Allouche, A.; Aycard, J.-P.; Rajzmann, M.; Hutschka, F., Study of γ-Alumina Surface Reactivity: Adsorption of Water and Hydrogen Sulfide on Octahedral Aluminum Sites. *The Journal of Physical Chemistry B* **2002,** 106, (36), 9359-9366.
19. Serbezov, A., Adsorption Equilibrium of Water Vapor on F-200 Activated Alumina. *J. Chem. Eng. Data* **2003,** 48, (2), 421-425.
20. Borello, E., Surface rehydration of variously dehydrated eta-alumina. *J. Catal.* **1974,** 35, (1), 1-10.
21. Altarawneh, M.; Assaf, N. W.; Hussain, H. M.; Dlugogorski, B. Z., Structural properties of alumina surfaces and their roles in the synthesis of environmentally persistent free radicals (EPFRs). *Nanotechnology Reviews* **2023,** 12, (1).
22. Kozerozhets, I. V.; Semenov, E. A.; Avdeeva, V. V.; Ivakin, Y. D.; Kupreenko, S. Y.; Egorov, A. V.; Kholodkova, A. A.; Vasil'ev, M. G.; Kozlova, L. O.; Panasyuk, G. P., State and forms of water in dispersed aluminum oxides and hydroxides. *Ceram. Int.* **2023,** 49, (18), 30381-30394.
23. Brunauer, S.; Emmett, P. H.; Teller, E., Adsorption of Gases in Multimolecular Layers. *J. Am. Chem. Soc.* **1938,** 60, (2), 309-319.
24. Thommes, M.; Kaneko, K.; Neimark, A. V.; Olivier, J. P.; Rodriguez-Reinoso, F.; Rouquerol, J.; Sing, K. S. W., Physisorption of gases, with special reference to the evaluation of surface area and pore size distribution (IUPAC Technical Report). **2015**.
25. Al-Abadleh, H. A.; Grassian, V. H., FT-IR Study of Water Adsorption on Aluminum Oxide Surfaces. *Langmuir* **2003,** 19, (2), 341-347.
26. Xu, H.; Zhang, C.; Cai, J.; Wang, J.; Liu, K.; Cheng, X., Synthesis and characterization of activated alumina with high thermal stability by a low-heat solid-phase precursor method. *Microporous Mesoporous Mater.* **2022,** 337, 111921.
27. Wang, Q.; Li, W.; Hung, I.; Mentink-Vigier, F.; Wang, X.; Qi, G.; Wang, X.; Gan, Z.; Xu, J.; Deng, F., Mapping the oxygen structure of γ-Al2O3 by high-field solid-state NMR spectroscopy. *Nature Communications* **2020,** 11, (1), 3620.
28. Rui, Z.; Yan, Z.; Kai, H.; Zhen-ping, J.; Gong-zhen, C., NMR revealed activated alumina-water interaction. *Wuhan University Journal of Natural Sciences* **2005,** 10, (3), 572-576.
29. Thommes, M.; Kaneko, K.; Neimark, A. V.; Olivier, J. P.; Rodriguez-Reinoso, F.; Rouquerol, J.; Sing, K. S. W., Physisorption of gases, with special reference to the evaluation of surface area and pore size distribution (IUPAC Technical Report). *Pure Appl. Chem.* **2015,** 87, (9-10), 1051-1069.
30. Zubiaga, A.; Warringham, R.; Mitchell, S.; Gerchow, L.; Cooke, D.; Crivelli, P.; Pérez-Ramírez, J., Pore Topology Effects in Positron Annihilation Spectroscopy of Zeolites. *ChemPhysChem* **2017,** 18, (5), 470-479.
31. Warringham, R.; Gerchow, L.; Zubiaga, A.; Cooke, D.; Crivelli, P.; Mitchell, S.; Pérez-Ramírez, J., Insights into the Mechanism of Zeolite Detemplation by Positron Annihilation Lifetime Spectroscopy. *The Journal of Physical Chemistry C* **2016,** 120, (44), 25451-25461.
32. Milina, M.; Mitchell, S.; Cooke, D.; Crivelli, P.; Pérez-Ramírez, J., Impact of Pore Connectivity on the Design of Long-Lived Zeolite Catalysts. *Angewandte Chemie International Edition* **2015,** 54, (5), 1591-1594.
33. Urban-Klaehn, J.; Shikhaliyev, K.; Gaffney, A.; Martinez, A.; Zaleski, R.; Lauterbach, J.; Katz, A.; Jaeshke, A.; Li, X., Zeolite-Based Catalysts for Conversion of Oxygenated Polymer Waste by Positron Annihilation. *ChemCatChem* **2024,** 16, (4), e202301282.
34. Attallah, A. G.; Bon, V.; Maity, K.; Hirschmann, E.; Butterling, M.; Wagner, A.; Kaskel, S., Unravelling the Water Adsorption Mechanism in Hierarchical MOFs: Insights from In Situ Positron Annihilation Lifetime Studies. *ACS Applied Materials & Interfaces* **2023,** 15, (41), 48264-48276.
35. Zaleski, R.; Krasucka, P.; Skrzypiec, K.; Goworek, J., Macro- and Nanoscopic Studies of Porous Polymer Swelling. *Macromolecules* **2017,** 50, (13), 5080-5089.

 doi:10.20944/preprints202507.0193.v1

36. Kierys, A.; Zaleski, R.; Grochowicz, M.; Gorgol, M.; Sienkiewicz, A., Polymer–mesoporous silica composites for drug release systems. *Microporous Mesoporous Mater.* **2020,** 294, 109881.
37. Zaleski, R.; Błażewicz, A.; Kierys, A., Ortho-positronium migration in mesopores of MCM-41, MSF and SBA-3. *Nukleonika* **2013,** 58, (1), 233−238.
38. Zaleski, R.; Gorgol, M.; Kierys, A.; Goworek, J., Positron porosimetry study of mesoporous polymer–silica composites. *Adsorption* **2016,** 22, (4), 745-754.
39. Lupa, J.; Gorgol, M.; Greluk, M.; Rotko, M.; Słowik, G.; Zaleski, R.; Kierys, A., Toward Understanding the Reduction Process of Nickel Oxide and Ceria-Based Nickel Catalyst via Positron Annihilation Lifetime Spectroscopy. *The Journal of Physical Chemistry C* **2025,** 129, (25), 11355-11364.
40. Zaleski, R.; Kierys, A.; Pietrow, M.; Zgardzińska, B.; Błażewicz, A., Influence of different confining matrices on negative pressure in liquid n-heptane investigated using positronium bubbles as a probe. *J. Colloid Interface Sci.* **2020,** 558, 259-268.
41. Kierys, A.; Zaleski, R.; Tydda, M.; Goworek, J., What can positronium tell us about adsorption? *Adsorption* **2013,** 19, (2-4), 529-535.
42. Kierys, A.; Zaleski, R.; Gorgol, M.; Goworek, J., N-Heptane adsorption in periodic mesoporous silica by in situ positron annihilation lifetime spectroscopy. *Microporous Mesoporous Mater.* **2013,** 179, 104-110.
43. Attallah, A. G.; Bon, V.; Hirschmann, E.; Butterling, M.; Wagner, A.; Zaleski, R.; Kaskel, S., Uncovering the Dynamic CO2 Gas Uptake Behavior of CALF-20 (Zn) under Varying Conditions via Positronium Lifetime Analysis. *Small* **2025,** 21, (14), 2500544.
44. Stuart, N. M.; Sohlberg, K., The Microstructure of γ-Alumina. *Energies* **2021,** 14, (20), 6472.
45. Compalox® activated aluminum oxides. https://chembase-st.com/wp-content/uploads/Compalox-Activated-Aluminum-Oxides-for-Sustainability.pdf (12.06.2025),
46. Becvár, F., Methodology of positron lifetime spectroscopy: Present status and perspectives. *Nucl. Instrum. Methods Phys. Res., Sect. B* **2007,** 261, (1-2), 871-874.
47. Kansy, J., Microcomputer program for analysis of positron annihilation lifetime spectra. *Nucl. Instrum. Methods Phys. Res., Sect. A* **1996,** 374, (2), 235-244.
48. Shukla, A.; Peter, M.; Hoffmann, L., Analysis of positron lifetime spectra using quantified maximum entropy and a general linear filter. *Nucl. Instrum. Methods Phys. Res., Sect. A* **1993,** 335, (1-2), 310-317.
49. Zaleski, R., Principles of positron porosimetry. *Nukleonika* **2015,** 60, (4), 795-800.
50. Vorobiev, J. K.; Badaev, B. N.; Ljubushko, G. I.; Levitsky, E. A.; Boreskov, G. K.; Andrushkevich, M. M.; Baum, B. A.; Pakhomov, N. A.; Khomyakova, L. G.; Khramov, A. E.; Rodionova, N. A.; Isaev, B. N.; Knyazev, V. M.; Moroz, E. M.; Erofeev, V. N.; Druzhinin, I. P.; Shkrabina, R. A. Method of preparing granulated activated alumina US Patent 4,166,100, filled 1978-05-26, and issued 1979-08-28.
51. Loarer, J.-L. L.; Nussbaum, H.; Bortzmeyer, D. Alumina extrudates, methods for preparing and use as catalysts supports. US Patent 6,656,875 B1, filled 1998-06-10, and issued 2003-12-02.
52. Chopin, T.; Fourre, P.; Jaeger, P.; Taxil, B. Crush resistant adsorptive agglomerates of activated alumina. US Patent 5,637,547, filled 1995-09-22, and issued 1997-06-10.
53. Zhou, R.-S.; Snyder, R. L., Structures and transformation mechanisms of the [eta], [gamma] and [theta] transition aluminas. *Acta Crystallographica Section B* **1991,** 47, (5), 617-630.
54. van Gog, H., First-principles study of dehydration interfaces between diaspore and corundum, gibbsite and boehmite, and boehmite and γ-Al2O3: Energetic stability, interface charge effects, and dehydration defects. *Appl. Surf. Sci.* **2021,** 541, 148501.
55. Prins, R., On the structure of γ-Al2O3. *J. Catal.* **2020,** 392, 336-346.
56. Thommes, M.; Kaneko, K.; Neimark Alexander, V.; Olivier James, P.; Rodriguez-Reinoso, F.; Rouquerol, J.; Sing Kenneth, S. W., Physisorption of gases, with special reference to the evaluation of surface area and pore size distribution (IUPAC Technical Report). In *Pure Appl. Chem.*, 2015; Vol. 87, p 1051.
57. Gorgol, M.; Tydda, M.; Kierys, A.; Zaleski, R., Composition of pore surface investigated by positron annihilation lifetime spectroscopy. *Microporous Mesoporous Mater.* **2012,** 163, (0), 276-281.
58. Thraenert, S.; Hassan, E. M.; Enke, D.; Fuerst, D.; Krause-Rehberg, R., Verifying the RTE model: ortho-positronium lifetime measurement on controlled pore glasses. *Phys. Status Solidi C* **2007,** 4, (10), 3819-3822.

 doi:10.20944/preprints202507.0193.v1

59. Consolati, G.; Quasso, F., Positronium dynamics in aqueous solutions of ionic surfactants. *Chem. Phys.* **1996,** 213, (1-3), 449-457.
60. Murakami, H.; Endo, T.; Matsuda, I., Positron lifetime in voids induced in quenched aluminum. *Phys. Rev. B: Condens. Matter Mater. Phys.* **1991,** 44, (6), 2504-2506.
61. Zaleski, R.; Kotowicz, O.; Górska, A.; Zaleski, K.; Zgardzińska, B., Investigation of the Ability to Detect Electrolyte Disorder Using PET with Positron Annihilation Lifetime Spectroscopy. *The Journal of Physical Chemistry B* **2023,** 127, (46), 9887-9890.
62. Stepanov, S. V.; Byakov, V. M.; Duplâtre, G.; Zvezhinskiy, D. S.; Lomachuk, Y. V., Positronium formation in a liquid phase: Influence of intratrack reactions and temperature. *Phys. Status Solidi C* **2009,** 6, (11), 2476-2481.
63. Stepanov, S. V.; Byakov, V. M.; Hirade, T., To the theory of Ps formation. New interpretation of the e+ lifetime spectrum in water. *Radiat. Phys. Chem.* **2007,** 76, (2), 90-95.
64. Zaleski, R.; Gorgol, M.; Kierys, A.; Maheshwari, P.; Pietrow, M.; Pujari, P. K.; Zgardzińska, B., Unraveling the Phase Behavior of Water Confined in Nanochannels through Positron Annihilation. *The Journal of Physical Chemistry C* **2022,** 126, (13), 5916-5926.
65. Ferrell, R. A., Long Lifetime of Positronium in Liquid Helium. *Phys. Rev.* **1957,** 108, (2), 167-168.
66. Maheshwari, P.; Gorgol, M.; Kierys, A.; Zaleski, R., Positron Probing of Liquid-free Volume To Investigate Adsorption–Desorption Behavior of Water in Two-Dimensional Mesoporous SBA-3. *J. Phys. Chem. C* **2017,** 121, (32), 17251-17262.
67. Zaleski, R., Measurement and Analysis of the Positron Annihilation Lifetime Spectra for Mesoporous Silica. *Acta Phys. Polon. A* **2006,** 110, (5), 729-738.
68. Gorgol, M.; Krasucka, P.; Goworek, J.; Zaleski, R., Controlled Porosity of MCM-41 Obtained by Partial Blocking of Pores by Silicon Oil. *Acta Phys. Polon. A* **2017,** 132, (5), 1559-1563.
69. Zaleski, R.; Gorgol, M.; Błazewicz, A.; Kierys, A.; Goworek, J., N-heptane adsorption and desorption in mesoporous materials. *Journal of Physics: Conference Series* **2015,** 618, (1), 012040.